

Measurement of the Inelastic Proton-Proton Cross-Section at $\sqrt{s} \geq 40$ TeV Using the Hybrid Data of the Pierre Auger Observatory

Olena Tkachenko^{a,*} for the Pierre Auger Collaboration^b

^a*Institute of Physics of the Czech Academy of Sciences, Na Slovance 1999/2, 182 00 Prague, Czech Republic*

^b*Observatorio Pierre Auger, Av. San Martín Norte 304, 5613 Malargüe, Argentina*

Full author list: https://www.auger.org/archive/authors_icrc_2025.html

E-mail: spokespersons@auger.org

Measuring proton-proton interaction cross-sections at center-of-mass energies above 40 TeV remains a significant challenge in particle physics. The Pierre Auger Observatory provides a unique opportunity to study the interactions at the highest energies through the distribution of the depth of maximum shower development (X_{\max}) observed by its Fluorescence Detector. In previous studies, the determination of the interaction cross-section at ultrahigh energies has relied on the assumption that the tail of the X_{\max} distribution is proton-dominated, which restricts the analysis to a limited energy range below the ankle and introduces related systematic uncertainties. In this contribution, we adopt a novel method for the simultaneous estimation of the proton-proton interaction cross-section and the primary cosmic-ray mass composition using data from the Pierre Auger Observatory, avoiding assumptions about one quantity to infer the other and thus improving the accuracy and robustness of our analysis. In addition, a systematic shift in the X_{\max} scale is fitted to account for both experimental uncertainties and theoretical constraints on the modeling of particle interactions. The obtained results are consistent with previous analyses and provide additional constraints on hadronic interaction models. The measured proton-proton inelastic cross-section at ultra-high energies agrees well with extrapolations of accelerator data. The inferred cosmic-ray composition and the X_{\max} -scale shift are also compatible with previous estimates.

*Speaker

1. Introduction

A key observable in the studies of ultrahigh-energy cosmic rays (UHECRs) is the atmospheric depth at which the air shower reaches its maximum development, denoted X_{\max} . This quantity is highly sensitive to both the mass composition of the primary cosmic rays and the hadronic interaction properties of the shower development. Specifically, X_{\max} scales with the logarithm of the mass of the primary particle, providing information on its nuclear mass while also reflecting the depth of the first atmospheric interaction, which depends on the interaction cross-section of the incoming particle with air nuclei. However, at ultrahigh energies, neither the mass composition nor the hadronic cross-sections are directly or precisely measured, and estimating one often requires assumptions about the other. This mutual dependence is further complicated by the fact that the X_{\max} scale itself is not well constrained by current hadronic interaction models [1], introducing additional uncertainty into the interpretation of both observables.

Addressing these interconnected uncertainties is critical. Studies of the mass composition help constrain the possible astrophysical sources of UHECRs, while probing hadronic interactions at these extreme energies offers insight into soft QCD processes that are well beyond the reach of human-made accelerators. Traditionally, measurements of the proton-air or proton-proton cross-sections, which is central to constraining hadronic models, have relied on the assumption that the tail of the X_{\max} distribution is dominated by protons, with a given helium contribution treated as a systematic uncertainty (typically limited to $\sim 25\%$) [2, 3]. Simultaneously, predictions of the mass composition rely on the same interaction models, making accurate cross-section estimates essential.

In this contribution, we refine the measurement of the proton-proton interaction cross-section through a simultaneous fit of the cross-section, mass composition, and X_{\max} scale using the data collected by the Fluorescence Detector (FD) of the Pierre Auger Observatory between December 1, 2004, and December 31, 2021 [4]. With this improved approach, we address the drawbacks of separate analyses and achieve a consistent estimation of the mass composition, the proton-proton interaction cross-section, and the X_{\max} scale while reducing reliance on the assumptions used in standard analyses.

2. Method

We determine the proton-proton interaction cross-section and UHECR mass composition through a simultaneous fit to the full X_{\max} distribution [5, 6], using predictions from air shower simulations with modified hadronic interaction properties. This approach builds on the standard mass composition fit [7], using the same data selection procedure, with updates to both the selection and the reconstruction of the longitudinal air shower profile detailed in [4, 8]. A further extension to the analysis is made by incorporating model predictions with modified interaction cross-sections. Additionally, it allows the X_{\max} scale to vary freely, accounting for associated experimental and theoretical uncertainties. The proton-proton cross-section is rescaled by introducing an energy-dependent factor f_{igE_1} , following the approach used in the original cross-section analysis by the Pierre Auger Collaboration [2, 9]. The modifications are implemented within the SIBYLL 2.3d model [10] using the CONEX air shower simulation code [11]. Due to the E/A scaling characteristic of the superposition model, the effective onset of cross-section modifications is shifted to

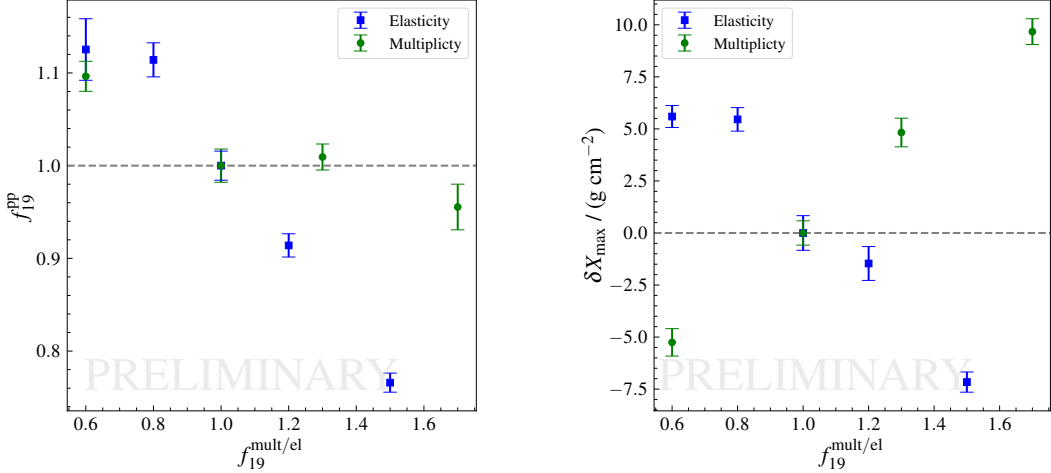


Figure 1: Biases in the fitted cross-section rescaling factor f_{19}^{pp} (left) and shift in the X_{\max} scale δX_{\max} (right) resulting from deviations in elasticity and multiplicity from the values assumed in the model prediction.

higher energies for nuclei with larger mass numbers. Consistently with the original analysis, the reference energy E_1 is fixed at 10^{19} eV, which defines the energy at which the rescaling factor reaches the constant parameter value f_{19}^{pp} . The threshold energy, above which the modifications in the cross-section are implemented, is set at the LHC center-of-mass energy. The nucleus-air cross-sections, calculated within the modified hadronic interaction model, are obtained via Glauber theory from the modified proton-proton cross-sections [12].

First, X_{\max} distribution templates, i.e., precomputed simulated distributions used for comparison with data, are generated for discrete values of the rescaling factor f_{19}^{pp} , ranging from 0.2 to 2.0 in steps of 0.1. For each value of f_{19}^{pp} , an X_{\max} template that includes the detector acceptance and resolution effects is produced. Independently, a shift in X_{\max} , denoted δX_{\max} , is applied to the data. This results in a two-dimensional scan over $(f_{19}^{\text{pp}}, \delta X_{\max})$, yielding a best-fit mass composition for each parameter pair. The quality of the fit is assessed using the deviance, defined as the logarithm of the Poisson likelihood, which is approximately χ^2 -distributed. We identify the values of f_{19}^{pp} and δX_{\max} that minimize the total χ^2 across all energy bins, assuming both parameters are energy-independent. This analysis assumes a mass-independent X_{\max} -scale shift. A fit including a $\ln A$ -dependent term showed no significant mass dependence, with the coefficient consistent with zero.

3. Uncertainties and Biases

Beyond statistical uncertainties, we account for relevant systematic effects, including those related to the energy scale, detector response, and hadronic interaction properties, specifically multiplicity and elasticity, as well as energy-dependent X_{\max} systematics. Detector and energy scale systematics are evaluated via Monte Carlo simulations incorporating the detector response of the Pierre Auger Observatory [13], following the standard X_{\max} mass composition analysis [7]. Uncertainties from extrapolating accelerator measurements of elasticity and multiplicity are assessed using CONEX simulations, with these parameters being modified by following the same approach as for the cross-section variations [9, 14]. The modified simulations are then refitted. In Figure 1,

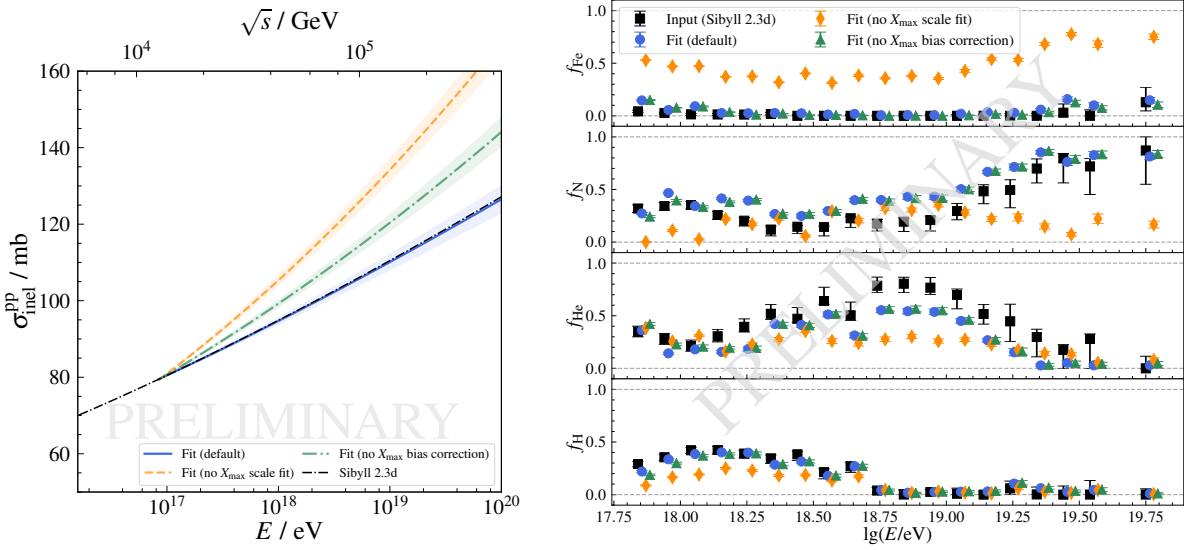


Figure 2: Validation of the fitting procedure on the simulations. Left: Proton-proton cross-section. Right: Fitted composition fractions. To illustrate the impact of the discussed biases, results are additionally presented for fits performed with a fixed X_{\max} scale and without applying the correction for the X_{\max} bias.

the resulting biases in the estimated cross-section and X_{\max} scale are shown. The largest deviations observed in f_{19}^{pp} , δX_{\max} , and the associated fractions are reported as systematic uncertainties.

The X_{\max} scale is affected by several systematic sources, primarily reconstruction effects at low energies and atmospheric variations at high energies [15]. Although these contributions combine to produce a nearly constant total uncertainty, their energy dependence can introduce both a global offset and an energy-dependent bias. To incorporate these dependencies, we generate multiple realizations of correlated X_{\max} shifts across energy bins by random sampling within the uncertainty ranges of each source, preserving their energy correlations.

A potentially overlooked factor in X_{\max} -based analyses is a reconstruction bias that depends on the X_{\max} value itself. Monte Carlo simulations show that both the mean and width of the difference between generated and reconstructed X_{\max} increase with larger X_{\max} , biasing the distribution tail by up to 15 g cm^{-2} . Since the tail is sensitive to interaction properties, this bias can significantly affect the fitted cross-section, while the central part remains stable with minimal bias. Because true X_{\max} values are unknown, the correction is applied to simulation templates by adjusting the double-Gaussian resolution parameters. The bias is modeled as a cubic function of X_{\max} and energy. It mainly affects the tail, with negligible impact on the mass composition, but it can bias the cross-section estimate by up to 10%, thus, correcting for it is essential for accurate cross-section determination. It is important to note that this bias, if present, also impacts the previously adopted method of measuring cross-sections from the tail of the X_{\max} distribution, with its extent depending on the profile reconstruction method. Neglecting this bias leads to an underestimation of Λ_η , which consequently causes an overestimation of the cross-section. Therefore, applying the X_{\max} -dependent correction is essential for both approaches.

Unlike the standard method, which infers the interaction cross-section from the tail of the X_{\max} distribution, the simultaneous fit of cross-section and mass composition yields an almost

unbiased estimate that is largely independent of the helium fraction or overall mass composition, as demonstrated previously [6]. In Figure 2, we show the fit results for simulations generated using the composition observed in the Pierre Auger Observatory data and incorporating the detector response. A negative 30 g cm^{-2} shift in the X_{\max} scale was included to test the impact of an unaccounted deviation from the SIBYLL 2.3d model. For comparison, the fit without correcting the X_{\max} -dependent bias is also shown. When both the scale shift and bias correction are applied, the reconstructed values agree well with the simulated inputs, including composition, X_{\max} shift, and cross-section. Small residual bias of approximately 6 g cm^{-2} in X_{\max} scale and an offset in composition are corrected in the fitted fractions and accounted for as systematic uncertainties in f_{19}^{pp} and δX_{\max} . If the X_{\max} shift is omitted from the fit, the cross-section is overestimated, and the composition is biased toward lighter elements, as the fit compensates for the differing X_{\max} scale by adjusting the shape of the distribution.

4. Results

We applied the fit procedure described above to the most recent data of the Pierre Auger Observatory, obtaining the cross-section, mass composition, and shift in the X_{\max} scale. These results are then compared to those from the standard mass composition fit, the cross-section derived from the tail of the X_{\max} distribution, and the latest Auger study evaluating hadronic model predictions for the X_{\max} scale.

In Figure 3, we show the two-dimensional scan over the cross-section rescaling factor and the shift in X_{\max} , from which the best-fit values of both parameters are determined. The displayed contours correspond to 68% confidence intervals, obtained using a profile likelihood method based on the $\chi^2 - \chi^2_{\min} = 1$ criterion. In Figure 4, the estimated cross-sections are presented, while in Figure 5, we show the corresponding mass composition. Both observables are compared to the predictions from the original (unmodified) SIBYLL 2.3d model, as well as to those

from the recently released EPOS LHC-R [16] and QGSJET-III.01 [17] hadronic interaction models. The estimated rescaling factor is $f_{19}^{\text{pp}} = 0.97^{+0.09}_{-0.07} (\text{stat.})^{+0.24}_{-0.18} (\text{syst.})$, and the corresponding shift in the X_{\max} scale is $\delta X_{\max} = -10.3^{+1.7}_{-1.5} (\text{stat.})^{+13.6}_{-14.3} (\text{syst.}) \text{ g cm}^{-2}$. The quoted systematic uncertainties account for the components and biases discussed in the previous section. Although the measured cross-section and X_{\max} values deviate from the predictions of the unmodified SIBYLL 2.3d model, they remain consistent within the total uncertainty. Notably, the direction of the observed deviations aligns with the trend predicted by the EPOS LHC-R model, which suggests a lower cross-section and a deeper X_{\max} compared to SIBYLL 2.3d. The comparison with the cross-sections derived from

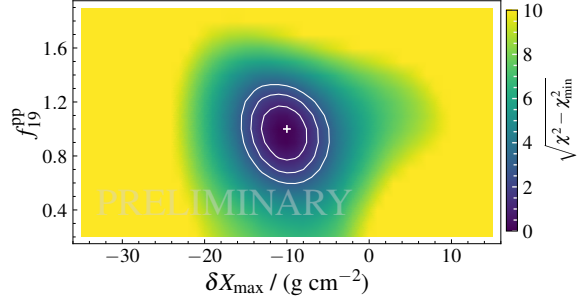


Figure 3: χ^2 contour of the fit, with the x -axis showing the X_{\max} -scale shift and the y -axis the cross-section rescaling factor. The color scale represents the difference between the χ^2 value at each parameter point and the minimum χ^2 value across the full parameter space, with contours indicating the confidence levels.

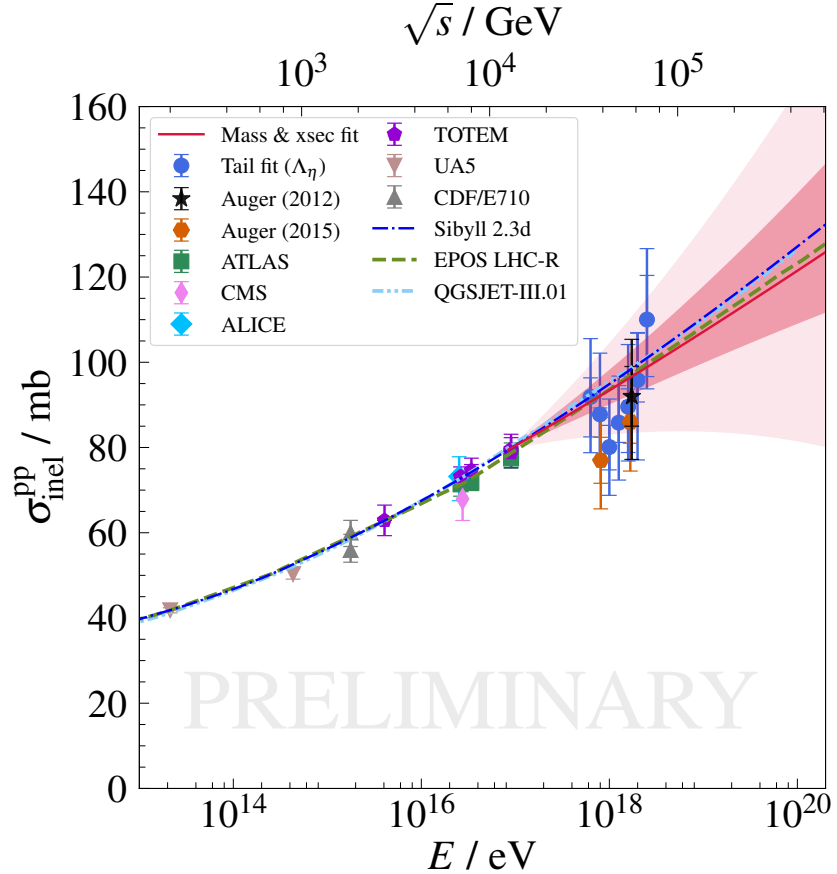


Figure 4: The inelastic proton-proton cross-section estimated from Pierre Auger Observatory data with a simultaneous fit of mass composition, cross-section and a shift in X_{\max} scale. The results are compared with predictions from contemporary hadronic interaction models, accelerator data, and measurements derived from the tail of the X_{\max} distribution. The darker shaded band indicates the statistical uncertainty, while the lighter band represents the total uncertainty.

the tail of the X_{\max} distribution shows good agreement in the energy range where the relative helium fraction remains sufficiently low for the tail method to provide reliable estimates.

The overall X_{\max} -scale shift obtained here is about 20 g cm^{-2} smaller than the one reported in the $(S(1000), X_{\max})$ analysis [1]. However, it is worth noting that the results presented in these proceedings depend on the selected energy range. Restricting our fit to the same energy interval used in that study yields a shift of $\delta X_{\max} = -15.6^{+2.2}_{-3.2} \text{ (stat.)}^{+13}_{-18} \text{ (syst.) g cm}^{-2}$, consistent within systematic uncertainties with the previously reported shift in the model predictions. The rescaling factor $f_{19}^{\text{pp}} = 0.74^{+0.14}_{-0.18} \text{ (stat.)}$ suggests an additional negative shift and broader X_{\max} distribution. Differences in energy range and analysis assumptions, however, complicate a direct comparison between the two analyses.

Relative to the composition-only fit with SIBYLL 2.3d, the mass composition obtained from the simultaneous composition and cross-section fit is heavier, yet still lighter than that predicted by EPOS LHC-R. In comparison with the unmodified SIBYLL 2.3d model, the proton and iron fractions remain nearly unchanged across most of the energy range, except at the highest energies

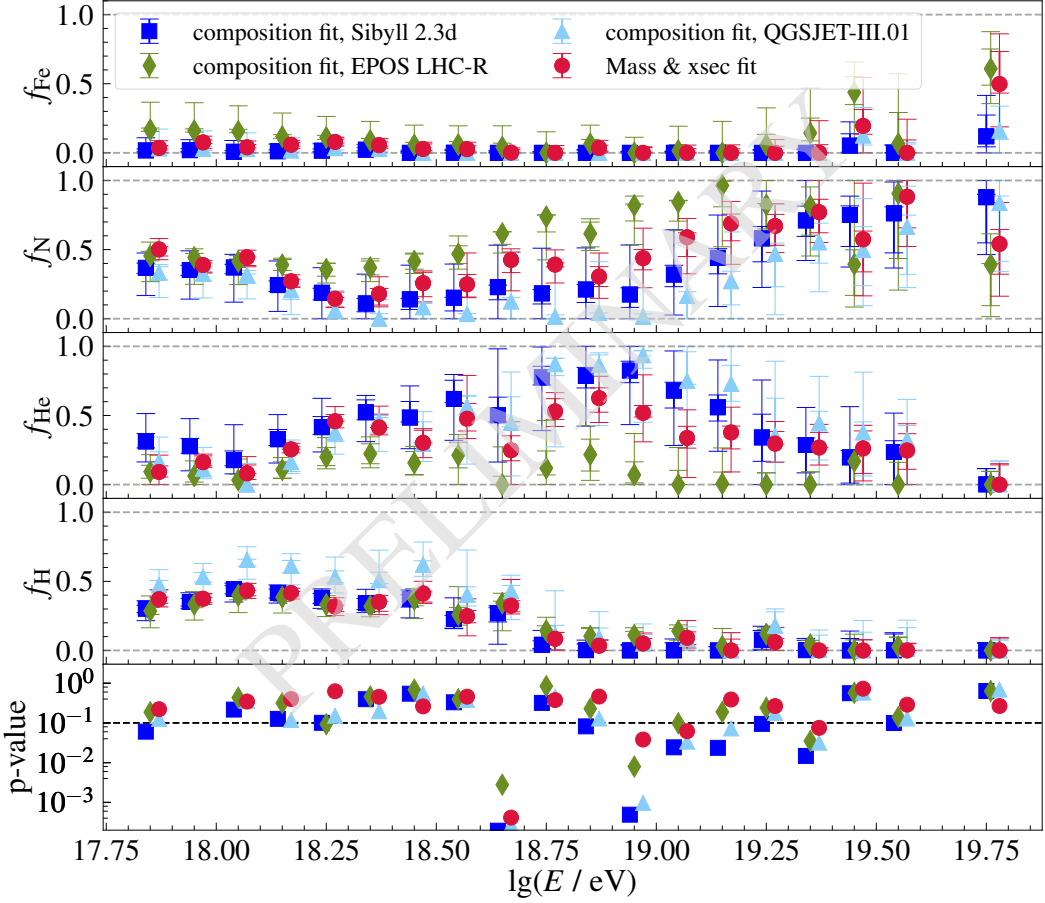


Figure 5: The mass composition estimated from Pierre Auger Observatory data with a simultaneous fit of mass composition, cross-section and a shift in X_{\max} scale. The results are compared with predictions from the composition-only fit using the predictions of the unmodified SIBYLL 2.3d, EPOS LHC-R, and QGSJET-III.01 interaction models. The inner caps represent statistical uncertainties, while the outer caps indicate the total uncertainties, including both statistical and systematic contributions. The bottom panel displays the quality of the fit.

where the iron fraction increases by up to 40%. The nitrogen and helium fractions, on the other hand, show more noticeable deviations from the unmodified SIBYLL 2.3d model, with the nitrogen fraction increasing by up to 20% in the intermediate energy range, accompanied by a corresponding decline in helium contamination. Overall, the new composition sits between the SIBYLL 2.3d and EPOS LHC-R predictions and remains compatible with both within the quoted total uncertainties. The improved agreement between the model and the data is reflected in the higher p-values, as shown in the bottom panel of Figure 5.

5. Conclusions

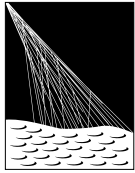
In this work, we present a joint analysis of the cosmic-ray mass composition and the inelastic proton-proton cross-section using the full Phase I dataset from the Pierre Auger Observatory. Both quantities are extracted via a simultaneous fit to the X_{\max} distributions, with the X_{\max} scale included

as a free parameter to address uncertainties in detector response and hadronic interaction models. This integrated approach reduces dependence on fixed assumptions, such as a proton-dominated X_{\max} tail or fixed model predictions, enhancing the internal consistency of the analysis. Compared to previous measurements, the statistical uncertainty on the proton-proton cross-section has decreased by about 20%, thanks to the larger dataset and methodological improvements. Systematic uncertainties are also lowered by incorporating dominant error sources directly into the fit. The applied method additionally improves the reliability of mass fraction estimates by explicitly including the proton-proton cross-section, which significantly contributes to model-related uncertainties, within the simultaneous fit. These advances enable a more precise and robust characterization of mass composition and cross-section, allowing for the extension of cross-section measurements to higher energies with reduced bias from heavier primaries, such as helium. The results obtained in this work suggest a somewhat heavier mass composition, a slightly lower proton-proton cross-section, and a small negative shift in the data relative to model predictions. In summary, the estimated proton-proton interaction cross-section, as well as the mass composition and the X_{\max} scale, remain consistent with previous measurements and theoretical model extrapolations within the quoted systematic uncertainties. This agreement supports the validity of the previous and current analyses while acknowledging the existing uncertainties and limitations inherent in the data and models.

References

- [1] A. Aab *et al.* [Pierre Auger Collaboration], *Phys. Rev. D* **109** (2024) 102001.
- [2] P. Abreu *et al.* [Pierre Auger Collaboration], *Phys. Rev. Lett.* **109** (2012) 062002.
- [3] R. Ulrich [for the Pierre Auger Collaboration], *PoS ICRC2015* (2015) 401.
- [4] T. Fitoussi [for the Pierre Auger Collaboration], *PoS UHECR2024* (2025) 041.
- [5] O. Tkachenko *et al.*, *PoS ICRC2021* (2021) 438.
- [6] O. Tkachenko [for the Pierre Auger Collaboration], *PoS UHECR2024* (2025) 036.
- [7] A. Aab *et al.* [Pierre Auger Collaboration], *Phys. Rev. D* **90** (2014) 122006.
- [8] J. Bellido [for the Pierre Auger Collaboration], *PoS ICRC2023* (2023) 211.
- [9] R. Ulrich, R. Engel, and M. Unger, *Phys. Rev. D* **83** (2011) 054026.
- [10] F. Riehn *et al.*, *Phys. Rev. D* **102** (2020) 063002.
- [11] T. Bergmann *et al.*, *Astropart. Phys.* **26** (2007) 420.
- [12] R. J. Glauber, *Phys. Rev.* **100** (1955) 242.
- [13] E. Santos [for the Pierre Auger Collaboration], *PoS ICRC2023* (2023) 248.
- [14] J. Ebr *et al.*, *Ukr. J. Phys.* **11** (2024) 786.
- [15] A. Aab *et al.* [Pierre Auger Collaboration], *Phys. Rev. D* **90** (2014) 122005.
- [16] T. Pierog and K. Werner, *PoS ICRC2023* (2023) 230.
- [17] S. Ostapchenko, *Phys. Rev. D* **109** (2024) 094019.

The Pierre Auger Collaboration



PIERRE
AUGER
OBSERVATORY

- A. Abdul Halim¹³, P. Abreu⁷⁰, M. Aglietta^{53,51}, I. Allekotte¹, K. Almeida Cheminant^{78,77}, A. Almela^{7,12}, R. Aloisio^{44,45}, J. Alvarez-Muñiz⁷⁶, A. Ambrosone⁴⁴, J. Ammerman Yebra⁷⁶, G.A. Anastasi^{57,46}, L. Anchordoqui⁸³, B. Andrada⁷, L. Andrade Dourado^{44,45}, S. Andringa⁷⁰, L. Apollonio^{58,48}, C. Aramo⁴⁹, E. Arnone^{62,51}, J.C. Arteaga Velázquez⁶⁶, P. Assis⁷⁰, G. Avila¹¹, E. Avocone^{56,45}, A. Bakalova³¹, F. Barbato^{44,45}, A. Bartz Mocellin⁸², J.A. Bellido¹³, C. Berat³⁵, M.E. Bertaina^{62,51}, M. Bianciotto^{62,51}, P.L. Biermann^a, V. Binet⁵, K. Bismarck^{38,7}, T. Bister^{77,78}, J. Biteau^{36,i}, J. Blazek³¹, J. Blümer⁴⁰, M. Boháčová³¹, D. Boncioli^{56,45}, C. Bonifazi⁸, L. Bonneau Arbeletche²², N. Borodai⁶⁸, J. Brack^f, P.G. Brichetto Orchera^{7,40}, F.L. Briechle⁴¹, A. Bueno⁷⁵, S. Buitink¹⁵, M. Buscemi^{46,57}, M. Büskens^{38,7}, A. Bwembya^{77,78}, K.S. Caballero-Mora⁶⁵, S. Cabana-Freire⁷⁶, L. Caccianiga^{58,48}, F. Campuzano⁶, J. Caraça-Valente⁸², R. Caruso^{57,46}, A. Castellina^{53,51}, F. Catalani¹⁹, G. Cataldi⁴⁷, L. Cazon⁷⁶, M. Cerda¹⁰, B. Čermáková⁴⁰, A. Cermenati^{44,45}, J.A. Chinellato²², J. Chudoba³¹, L. Chytka³², R.W. Clay¹³, A.C. Cobos Cerutti⁶, R. Colalillo^{59,49}, R. Conceição⁷⁰, G. Consolati^{48,54}, M. Conte^{55,47}, F. Convenga^{44,45}, D. Correia dos Santos²⁷, P.J. Costa⁷⁰, C.E. Covault⁸¹, M. Cristinziani⁴³, C.S. Cruz Sanchez³, S. Dasso^{4,2}, K. Daumiller⁴⁰, B.R. Dawson¹³, R.M. de Almeida²⁷, E.-T. de Boone⁴³, B. de Errico²⁷, J. de Jesús⁷, S.J. de Jong^{77,78}, J.R.T. de Mello Neto²⁷, I. De Miti^{44,45}, J. de Oliveira¹⁸, D. de Oliveira Franco⁴², F. de Palma^{55,47}, V. de Souza²⁰, E. De Vito^{55,47}, A. Del Popolo^{57,46}, O. Deligny³³, N. Denner³¹, L. Deval^{53,51}, A. di Matteo⁵¹, C. Dobrigkeit²², J.C. D'Olivo⁶⁷, L.M. Domingues Mendes^{16,70}, Q. Dorosti⁴³, J.C. dos Anjos¹⁶, R.C. dos Anjos²⁶, J. Ebr³¹, F. Ellwanger⁴⁰, R. Engel^{38,40}, I. Epicoco^{55,47}, M. Erdmann⁴¹, A. Etchegoyen^{7,12}, C. Evoli^{44,45}, H. Falcke^{77,79,78}, G. Farrar⁸⁵, A.C. Fauth²², T. Fehler⁴³, F. Feldbusch³⁹, A. Fernandes⁷⁰, M. Fernandez¹⁴, B. Fick⁸⁴, J.M. Figueira⁷, P. Filip^{38,7}, A. Filipčič^{74,73}, T. Fitoussi⁴⁰, B. Flaggs⁸⁷, T. Fodran⁷⁷, A. Franco⁴⁷, M. Freitas⁷⁰, T. Fujii^{86,h}, A. Fuster^{7,12}, C. Galea⁷⁷, B. García⁶, C. Gaudu³⁷, P.L. Ghia³³, U. Giacconi⁴⁷, F. Gobbi¹⁰, F. Gollan⁷, G. Golup¹, M. Gómez Berisso¹, P.F. Gómez Vitale¹¹, J.P. Gongora¹¹, J.M. González¹, N. González⁷, D. Góra⁶⁸, A. Gorgi^{53,51}, M. Gottowik⁴⁰, F. Guarino^{59,49}, G.P. Guedes²³, L. Gützow⁴⁰, S. Hahn³⁸, P. Hamal³¹, M.R. Hampel⁷, P. Hansen³, V.M. Harvey¹³, A. Haungs⁴⁰, T. Hebbeker⁴¹, C. Hojvat^d, J.R. Hörandel^{77,78}, P. Horvath³², M. Hrabovsky³², T. Huege^{40,15}, A. Insolia^{57,46}, P.G. Isar⁷², M. Ismaiel^{77,78}, P. Janecek³¹, V. Jilek³¹, K.-H. Kampert³⁷, B. Keilhauer⁴⁰, A. Khakurdikar⁷⁷, V.V. Kizakke Covilakam^{7,40}, H.O. Klages⁴⁰, M. Kleifges³⁹, J. Köhler⁴⁰, F. Krieger⁴¹, M. Kubatova³¹, N. Kunka³⁹, B.L. Lago¹⁷, N. Langner⁴¹, N. Leal⁷, M.A. Leigui de Oliveira²⁵, Y. Lema-Capeans⁷⁶, A. Letessier-Selvon³⁴, I. Lhenry-Yvon³³, L. Lopes⁷⁰, J.P. Lundquist⁷³, M. Mallamaci^{60,46}, D. Mandat³¹, P. Mantsch^d, F.M. Mariani^{58,48}, A.G. Mariazzi³, I.C. Marić¹⁴, G. Marsella^{60,46}, D. Martello^{55,47}, S. Martinelli^{40,7}, M.A. Martins⁷⁶, H.-J. Mathes⁴⁰, J. Matthews^g, G. Matthiae^{61,50}, E. Mayotte⁸², S. Mayotte⁸², P.O. Mazur^d, G. Medina-Tanco⁶⁷, J. Meinert³⁷, D. Melo⁷, A. Menshikov³⁹, C. Merx⁴⁰, S. Michal³¹, M.I. Micheletti⁵, L. Miramonti^{58,48}, M. Mogarkar⁶⁸, S. Mollerach¹, F. Montanet³⁵, L. Morejon³⁷, K. Mulrey^{77,78}, R. Mussa⁵¹, W.M. Namasaka³⁷, S. Negi³¹, L. Nellen⁶⁷, K. Nguyen⁸⁴, G. Nicora⁹, M. Niechciol⁴³, D. Nitz⁸⁴, D. Nosek³⁰, A. Novikov⁸⁷, V. Novotny³⁰, L. Nožka³², A. Nucita^{55,47}, L.A. Núñez²⁹, J. Ochoa^{7,40}, C. Oliveira²⁰, L. Östman³¹, M. Palatka³¹, J. Pallotta⁹, S. Panja³¹, G. Parente⁷⁶, T. Paulsen³⁷, J. Pawlowsky³⁷, M. Pech³¹, J. Pěkala⁶⁸, R. Pelayo⁶⁴,

V. Pelgrims¹⁴, L.A.S. Pereira²⁴, E.E. Pereira Martins^{38,7}, C. Pérez Bertolli^{7,40}, L. Perrone^{55,47}, S. Petrera^{44,45}, C. Petrucci⁵⁶, T. Pierog⁴⁰, M. Pimenta⁷⁰, M. Platino⁷, B. Pont⁷⁷, M. Pourmohammadi Shahvar^{60,46}, P. Privitera⁸⁶, C. Priyadarshi⁶⁸, M. Prouza³¹, K. Pytel⁶⁹, S. Querchfeld³⁷, J. Rautenberg³⁷, D. Ravignani⁷, J.V. Reginatto Akim²², A. Reuzki⁴¹, J. Ridky³¹, F. Riehn^{76,j}, M. Risso⁴³, V. Rizi^{56,45}, E. Rodriguez^{7,40}, G. Rodriguez Fernandez⁵⁰, J. Rodriguez Rojo¹¹, S. Rossoni⁴², M. Roth⁴⁰, E. Roulet¹, A.C. Rovero⁴, A. Saftoiu⁷¹, M. Saharan⁷⁷, F. Salamida^{56,45}, H. Salazar⁶³, G. Salina⁵⁰, P. Sampathkumar⁴⁰, N. San Martin⁸², J.D. Sanabria Gomez²⁹, F. Sánchez⁷, E.M. Santos²¹, E. Santos³¹, F. Sarazin⁸², R. Sarmento⁷⁰, R. Sato¹¹, P. Savina^{44,45}, V. Scherini^{55,47}, H. Schieler⁴⁰, M. Schimassek³³, M. Schimp³⁷, D. Schmidt⁴⁰, O. Scholten^{15,b}, H. Schoorlemmer^{77,78}, P. Schovánek³¹, F.G. Schröder^{87,40}, J. Schulte⁴¹, T. Schulz³¹, S.J. Sciutto³, M. Scornavacche⁷, A. Sedoski⁷, A. Segreto^{52,46}, S. Sehgal³⁷, S.U. Shivashankara⁷³, G. Sigl⁴², K. Simkova^{15,14}, F. Simon³⁹, R. Šmídá⁸⁶, P. Sommers^e, R. Squartini¹⁰, M. Stadelmaier^{40,48,58}, S. Stanič⁷³, J. Stasielak⁶⁸, P. Stassi³⁵, S. Strähnz³⁸, M. Straub⁴¹, T. Suomijärvi³⁶, A.D. Supanitsky⁷, Z. Svozilíkova³¹, K. Syrokaš³⁰, Z. Szadkowski⁶⁹, F. Tairli¹³, M. Tambone^{59,49}, A. Tapia²⁸, C. Taricco^{62,51}, C. Timmermans^{78,77}, O. Tkachenko³¹, P. Tobiska³¹, C.J. Todero Peixoto¹⁹, B. Tomé⁷⁰, A. Travaini¹⁰, P. Travnicek³¹, M. Tueros³, M. Unger⁴⁰, R. Uzeiroska³⁷, L. Vaclavek³², M. Vacula³², I. Vaiman^{44,45}, J.F. Valdés Galicia⁶⁷, L. Valore^{59,49}, P. van Dillen^{77,78}, E. Varela⁶³, V. Vašíčková³⁷, A. Vásquez-Ramírez²⁹, D. Veberič⁴⁰, I.D. Vergara Quispe³, S. Verpoest⁸⁷, V. Verzi⁵⁰, J. Vicha³¹, J. Vink⁸⁰, S. Vorobiov⁷³, J.B. Vuta³¹, C. Watanabe²⁷, A.A. Watson^c, A. Weindl⁴⁰, M. Weitz³⁷, L. Wiencke⁸², H. Wilczyński⁶⁸, B. Wundheiler⁷, B. Yue³⁷, A. Yushkov³¹, E. Zas⁷⁶, D. Zavrtanik^{73,74}, M. Zavrtanik^{74,73}

— • —

¹ Centro Atómico Bariloche and Instituto Balseiro (CNEA-UNCuyo-CONICET), San Carlos de Bariloche, Argentina

² Departamento de Física and Departamento de Ciencias de la Atmósfera y los Océanos, FCEyN, Universidad de Buenos Aires and CONICET, Buenos Aires, Argentina

³ IFLP, Universidad Nacional de La Plata and CONICET, La Plata, Argentina

⁴ Instituto de Astronomía y Física del Espacio (IAFE, CONICET-UBA), Buenos Aires, Argentina

⁵ Instituto de Física de Rosario (IFIR) – CONICET/U.N.R. and Facultad de Ciencias Bioquímicas y Farmacéuticas U.N.R., Rosario, Argentina

⁶ Instituto de Tecnologías en Detección y Astropartículas (CNEA, CONICET, UNSAM), and Universidad Tecnológica Nacional – Facultad Regional Mendoza (CONICET/CNEA), Mendoza, Argentina

⁷ Instituto de Tecnologías en Detección y Astropartículas (CNEA, CONICET, UNSAM), Buenos Aires, Argentina

⁸ International Center of Advanced Studies and Instituto de Ciencias Físicas, ECyT-UNSAM and CONICET, Campus Miguelete – San Martín, Buenos Aires, Argentina

⁹ Laboratorio Atmósfera – Departamento de Investigaciones en Láseres y sus Aplicaciones – UNIDEF (CITEDEF-CONICET), Argentina

¹⁰ Observatorio Pierre Auger, Malargüe, Argentina

- ¹¹ Observatorio Pierre Auger and Comisión Nacional de Energía Atómica, Malargüe, Argentina
¹² Universidad Tecnológica Nacional – Facultad Regional Buenos Aires, Buenos Aires, Argentina
¹³ University of Adelaide, Adelaide, S.A., Australia
¹⁴ Université Libre de Bruxelles (ULB), Brussels, Belgium
¹⁵ Vrije Universiteit Brussels, Brussels, Belgium
¹⁶ Centro Brasileiro de Pesquisas Fisicas, Rio de Janeiro, RJ, Brazil
¹⁷ Centro Federal de Educação Tecnológica Celso Suckow da Fonseca, Petropolis, Brazil
¹⁸ Instituto Federal de Educação, Ciência e Tecnologia do Rio de Janeiro (IFRJ), Brazil
¹⁹ Universidade de São Paulo, Escola de Engenharia de Lorena, Lorena, SP, Brazil
²⁰ Universidade de São Paulo, Instituto de Física de São Carlos, São Carlos, SP, Brazil
²¹ Universidade de São Paulo, Instituto de Física, São Paulo, SP, Brazil
²² Universidade Estadual de Campinas (UNICAMP), IFGW, Campinas, SP, Brazil
²³ Universidade Estadual de Feira de Santana, Feira de Santana, Brazil
²⁴ Universidade Federal de Campina Grande, Centro de Ciencias e Tecnologia, Campina Grande, Brazil
²⁵ Universidade Federal do ABC, Santo André, SP, Brazil
²⁶ Universidade Federal do Paraná, Setor Palotina, Palotina, Brazil
²⁷ Universidade Federal do Rio de Janeiro, Instituto de Física, Rio de Janeiro, RJ, Brazil
²⁸ Universidad de Medellín, Medellín, Colombia
²⁹ Universidad Industrial de Santander, Bucaramanga, Colombia
³⁰ Charles University, Faculty of Mathematics and Physics, Institute of Particle and Nuclear Physics, Prague, Czech Republic
³¹ Institute of Physics of the Czech Academy of Sciences, Prague, Czech Republic
³² Palacky University, Olomouc, Czech Republic
³³ CNRS/IN2P3, IJCLab, Université Paris-Saclay, Orsay, France
³⁴ Laboratoire de Physique Nucléaire et de Hautes Energies (LPNHE), Sorbonne Université, Université de Paris, CNRS-IN2P3, Paris, France
³⁵ Univ. Grenoble Alpes, CNRS, Grenoble Institute of Engineering Univ. Grenoble Alpes, LPSC-IN2P3, 38000 Grenoble, France
³⁶ Université Paris-Saclay, CNRS/IN2P3, IJCLab, Orsay, France
³⁷ Bergische Universität Wuppertal, Department of Physics, Wuppertal, Germany
³⁸ Karlsruhe Institute of Technology (KIT), Institute for Experimental Particle Physics, Karlsruhe, Germany
³⁹ Karlsruhe Institute of Technology (KIT), Institut für Prozessdatenverarbeitung und Elektronik, Karlsruhe, Germany
⁴⁰ Karlsruhe Institute of Technology (KIT), Institute for Astroparticle Physics, Karlsruhe, Germany
⁴¹ RWTH Aachen University, III. Physikalisches Institut A, Aachen, Germany
⁴² Universität Hamburg, II. Institut für Theoretische Physik, Hamburg, Germany
⁴³ Universität Siegen, Department Physik – Experimentelle Teilchenphysik, Siegen, Germany
⁴⁴ Gran Sasso Science Institute, L’Aquila, Italy
⁴⁵ INFN Laboratori Nazionali del Gran Sasso, Assergi (L’Aquila), Italy
⁴⁶ INFN, Sezione di Catania, Catania, Italy
⁴⁷ INFN, Sezione di Lecce, Lecce, Italy

- ⁴⁸ INFN, Sezione di Milano, Milano, Italy
⁴⁹ INFN, Sezione di Napoli, Napoli, Italy
⁵⁰ INFN, Sezione di Roma “Tor Vergata”, Roma, Italy
⁵¹ INFN, Sezione di Torino, Torino, Italy
⁵² Istituto di Astrofisica Spaziale e Fisica Cosmica di Palermo (INAF), Palermo, Italy
⁵³ Osservatorio Astrofisico di Torino (INAF), Torino, Italy
⁵⁴ Politecnico di Milano, Dipartimento di Scienze e Tecnologie Aerospaziali , Milano, Italy
⁵⁵ Università del Salento, Dipartimento di Matematica e Fisica “E. De Giorgi”, Lecce, Italy
⁵⁶ Università dell’Aquila, Dipartimento di Scienze Fisiche e Chimiche, L’Aquila, Italy
⁵⁷ Università di Catania, Dipartimento di Fisica e Astronomia “Ettore Majorana“, Catania, Italy
⁵⁸ Università di Milano, Dipartimento di Fisica, Milano, Italy
⁵⁹ Università di Napoli “Federico II”, Dipartimento di Fisica “Ettore Pancini”, Napoli, Italy
⁶⁰ Università di Palermo, Dipartimento di Fisica e Chimica ”E. Segrè”, Palermo, Italy
⁶¹ Università di Roma “Tor Vergata”, Dipartimento di Fisica, Roma, Italy
⁶² Università Torino, Dipartimento di Fisica, Torino, Italy
⁶³ Benemérita Universidad Autónoma de Puebla, Puebla, México
⁶⁴ Unidad Profesional Interdisciplinaria en Ingeniería y Tecnologías Avanzadas del Instituto Politécnico Nacional (UPIITA-IPN), México, D.F., México
⁶⁵ Universidad Autónoma de Chiapas, Tuxtla Gutiérrez, Chiapas, México
⁶⁶ Universidad Michoacana de San Nicolás de Hidalgo, Morelia, Michoacán, México
⁶⁷ Universidad Nacional Autónoma de México, México, D.F., México
⁶⁸ Institute of Nuclear Physics PAN, Krakow, Poland
⁶⁹ University of Łódź, Faculty of High-Energy Astrophysics, Łódź, Poland
⁷⁰ Laboratório de Instrumentação e Física Experimental de Partículas – LIP and Instituto Superior Técnico – IST, Universidade de Lisboa – UL, Lisboa, Portugal
⁷¹ “Horia Hulubei” National Institute for Physics and Nuclear Engineering, Bucharest-Magurele, Romania
⁷² Institute of Space Science, Bucharest-Magurele, Romania
⁷³ Center for Astrophysics and Cosmology (CAC), University of Nova Gorica, Nova Gorica, Slovenia
⁷⁴ Experimental Particle Physics Department, J. Stefan Institute, Ljubljana, Slovenia
⁷⁵ Universidad de Granada and C.A.F.P.E., Granada, Spain
⁷⁶ Instituto Galego de Física de Altas Enerxías (IGFAE), Universidade de Santiago de Compostela, Santiago de Compostela, Spain
⁷⁷ IMAPP, Radboud University Nijmegen, Nijmegen, The Netherlands
⁷⁸ Nationaal Instituut voor Kernfysica en Hoge Energie Fysica (NIKHEF), Science Park, Amsterdam, The Netherlands
⁷⁹ Stichting Astronomisch Onderzoek in Nederland (ASTRON), Dwingeloo, The Netherlands
⁸⁰ Universiteit van Amsterdam, Faculty of Science, Amsterdam, The Netherlands
⁸¹ Case Western Reserve University, Cleveland, OH, USA
⁸² Colorado School of Mines, Golden, CO, USA
⁸³ Department of Physics and Astronomy, Lehman College, City University of New York, Bronx, NY, USA

⁸⁴ Michigan Technological University, Houghton, MI, USA

⁸⁵ New York University, New York, NY, USA

⁸⁶ University of Chicago, Enrico Fermi Institute, Chicago, IL, USA

⁸⁷ University of Delaware, Department of Physics and Astronomy, Bartol Research Institute, Newark, DE, USA

^a Max-Planck-Institut für Radioastronomie, Bonn, Germany

^b also at Kapteyn Institute, University of Groningen, Groningen, The Netherlands

^c School of Physics and Astronomy, University of Leeds, Leeds, United Kingdom

^d Fermi National Accelerator Laboratory, Fermilab, Batavia, IL, USA

^e Pennsylvania State University, University Park, PA, USA

^f Colorado State University, Fort Collins, CO, USA

^g Louisiana State University, Baton Rouge, LA, USA

^h now at Graduate School of Science, Osaka Metropolitan University, Osaka, Japan

ⁱ Institut universitaire de France (IUF), France

^j now at Technische Universität Dortmund and Ruhr-Universität Bochum, Dortmund and Bochum, Germany

Acknowledgments

The successful installation, commissioning, and operation of the Pierre Auger Observatory would not have been possible without the strong commitment and effort from the technical and administrative staff in Malargüe. We are very grateful to the following agencies and organizations for financial support:

Argentina – Comisión Nacional de Energía Atómica; Agencia Nacional de Promoción Científica y Tecnológica (ANPCyT); Consejo Nacional de Investigaciones Científicas y Técnicas (CONICET); Gobierno de la Provincia de Mendoza; Municipalidad de Malargüe; NDM Holdings and Valle Las Leñas; in gratitude for their continuing cooperation over land access; Australia – the Australian Research Council; Belgium – Fonds de la Recherche Scientifique (FNRS); Research Foundation Flanders (FWO), Marie Curie Action of the European Union Grant No. 101107047; Brazil – Conselho Nacional de Desenvolvimento Científico e Tecnológico (CNPq); Financiadora de Estudos e Projetos (FINEP); Fundação de Amparo à Pesquisa do Estado de Rio de Janeiro (FAPERJ); São Paulo Research Foundation (FAPESP) Grants No. 2019/10151-2, No. 2010/07359-6 and No. 1999/05404-3; Ministério da Ciência, Tecnologia, Inovações e Comunicações (MCTIC); Czech Republic – GACR 24-13049S, CAS LQ100102401, MEYS LM2023032, CZ.02.1.01/0.0/0.0/16_013/0001402, CZ.02.1.01/0.0/0.0/18_046/0016010 and CZ.02.1.01/0.0/0.0/17_049/0008422 and CZ.02.01.01/00/22_008/0004632; France – Centre de Calcul IN2P3/CNRS; Centre National de la Recherche Scientifique (CNRS); Conseil Régional Ile-de-France; Département Physique Nucléaire et Corpusculaire (PNC-IN2P3/CNRS); Département Sciences de l’Univers (SDU-INSU/CNRS); Institut Lagrange de Paris (ILP) Grant No. LABEX ANR-10-LABX-63 within the Investissements d’Avenir Programme Grant No. ANR-11-IDEX-0004-02; Germany – Bundesministerium für Bildung und Forschung (BMBF); Deutsche

Forschungsgemeinschaft (DFG); Finanzministerium Baden-Württemberg; Helmholtz Alliance for Astroparticle Physics (HAP); Helmholtz-Gemeinschaft Deutscher Forschungszentren (HGF); Ministerium für Kultur und Wissenschaft des Landes Nordrhein-Westfalen; Ministerium für Wissenschaft, Forschung und Kunst des Landes Baden-Württemberg; Italy – Istituto Nazionale di Fisica Nucleare (INFN); Istituto Nazionale di Astrofisica (INAF); Ministero dell’Università e della Ricerca (MUR); CETEMPS Center of Excellence; Ministero degli Affari Esteri (MAE), ICSC Centro Nazionale di Ricerca in High Performance Computing, Big Data and Quantum Computing, funded by European Union NextGenerationEU, reference code CN_00000013; México – Consejo Nacional de Ciencia y Tecnología (CONACYT) No. 167733; Universidad Nacional Autónoma de México (UNAM); PAPIIT DGAPA-UNAM; The Netherlands – Ministry of Education, Culture and Science; Netherlands Organisation for Scientific Research (NWO); Dutch national e-infrastructure with the support of SURF Cooperative; Poland – Ministry of Education and Science, grants No. DIR/WK/2018/11 and 2022/WK/12; National Science Centre, grants No. 2016/22/M/ST9/00198, 2016/23/B/ST9/01635, 2020/39/B/ST9/01398, and 2022/45/B/ST9/02163; Portugal – Portuguese national funds and FEDER funds within Programa Operacional Factores de Competitividade through Fundação para a Ciência e a Tecnologia (COMPETE); Romania – Ministry of Research, Innovation and Digitization, CNCS-UEFISCDI, contract no. 30N/2023 under Romanian National Core Program LAPLAS VII, grant no. PN 23 21 01 02 and project number PN-III-P1-1.1-TE-2021-0924/TE57/2022, within PNCDI III; Slovenia – Slovenian Research Agency, grants P1-0031, P1-0385, I0-0033, N1-0111; Spain – Ministerio de Ciencia e Innovación/Agencia Estatal de Investigación (PID2019-105544GB-I00, PID2022-140510NB-I00 and RYC2019-027017-I), Xunta de Galicia (CIGUS Network of Research Centers, Consolidación 2021 GRC GI-2033, ED431C-2021/22 and ED431F-2022/15), Junta de Andalucía (SOMM17/6104/UGR and P18-FR-4314), and the European Union (Marie Skłodowska-Curie 101065027 and ERDF); USA – Department of Energy, Contracts No. DE-AC02-07CH11359, No. DE-FR02-04ER41300, No. DE-FG02-99ER41107 and No. DE-SC0011689; National Science Foundation, Grant No. 0450696, and NSF-2013199; The Grainger Foundation; Marie Curie-IRSES/EPLANET; European Particle Physics Latin American Network; and UNESCO.